ADVANCED FUNCTIONAL MATERIALS
www.afm-journal.de

High-Performance and Scalable Organosilicon Membranes for Energy-Efficient Alcohol Purification

Tengyang Zhu, Dongchen Shen, Jiayu Dong, Huan Liu, Qing Xia, Song Li, Lu Shao, and Yan Wang**

The production of bio-alcohol is increasingly gaining international attention due to its potential as a viable alternative to fossil fuels and its ability to mitigate carbon dioxide emissions. However, the cost of bio-alcohol production is almost double that of fossil fuels, primarily because of the low yield of the purification process. Herein, a high-performance and scalable organosilicon membrane with high chain flexibility and controllable crosslinking density is developed for energy-efficient alcohol purification. The synthesized organosilicon membrane achieves an ultrahigh total flux (5.8 kg·m^{-2}·h^{-1}) with a comparable separation factor (8.7) for ethanol/water separation, outperforming most state-of-the-art polymer-based membranes. Integrated experiments and molecular dynamics simulations confirm that the ultrafast alcohol permeation of the membrane originates from its high chain flexibility, large fractional free volume, and weak interactions between feed molecules and membranes. The universal applicability of the low-crosslinking mechanism for the formation of high-performance organosilicon membranes is also validated. Moreover, its high efficiency and scalability in membrane production, along with the stability of the casting solution, offer promising prospects for industrial applications.

1. Introduction

International Energy Agency predicts that the consumption of bio-liquid fuel will reach 147 million tonnes by 2030, constituting ≈7% of the global road transport energy demand. In particular, bio-alcohols, with high energy density, environmental benignity, and good compatibility with existing infrastructure, hold great promise as viable alternatives to fossil fuels while mitigating carbon dioxide emissions.[1] However, the production cost of bio-alcohols from the fermentation broth is nearly double that of fossil fuels, primarily because of the low yield of the purification process.[1a] In response, extensive international efforts have been invested in reducing the cost of bio-alcohol purification.[2] In this context, the development of sustainable technologies and materials for the purification of bio-alcohols has become increasingly crucial, playing a vital role in addressing pressing energy-related and environmental challenges.[3]

Compared to established large-scale distillation-based technology for bio-alcohol purification,[4] membrane-based pervaporation is attracting increasing attention because of its energy efficiency and environmental friendliness.[5] In this approach, the membrane is the critical component, that determines high separation efficiency.[6] Organosilicon membranes, as benchmark organophilic membranes, are very promising for energy-efficient bio-alcohol purification in practical industrial applications.[7] However, current organosilicon membranes exhibit a relatively low permeate flux and suffer from an inherent trade-off between permeate flux and alcohol/water selectivity. These issues stem from their dense micro-structures and rigid molecular chains, resulting from high crosslinking densities, limiting their efficiency in energy-efficient applications.[8] Various strategies, such as designing new molecular structures,[9] introducing fillers,[3b,10] and optimizing the fabrication process,[11] have already been proposed to improve the alcohol purification efficiency of organosilicon membranes. Although current approaches can improve either permeate flux or selectivity to some extent, no method can simultaneously improve alcohol purification efficiency and selectivity while maintaining membrane fabrication facile, which is crucial for practical industrial applications. Consequently, the development of a controlled,

T. Zhu, J. Dong, H. Liu, Q. Xia, Y. Wang
Key Laboratory of Material Chemistry for Energy Conversion and Storage (Huazhong University of Science & Technology)
Ministry of Education
Wuhan 430074, China
E-mail: wangyan@hust.edu.cn
T. Zhu, J. Dong, H. Liu, Q. Xia, Y. Wang
Hubei Key Laboratory of Material Chemistry and Service Failure
School of Chemistry and Chemical Engineering
Huazhong University of Science & Technology
Wuhan 430074, China
D. Shen, S. Li
Department of New Energy Science and Engineering
School of Energy and Power Engineering
Huazhong University of Science & Technology
Wuhan 430074, China
E-mail: songli@hust.edu.cn
L. Shao
State Key Laboratory of Urban Water Resource and Environment
School of Chemistry and Chemical Engineering
Harbin Institute of Technology
Harbin 150001, China

The ORCID identification number(s) for the author(s) of this article can be found under https://doi.org/10.1002/adfm.202415386

DOI: 10.1002/adfm.202415386

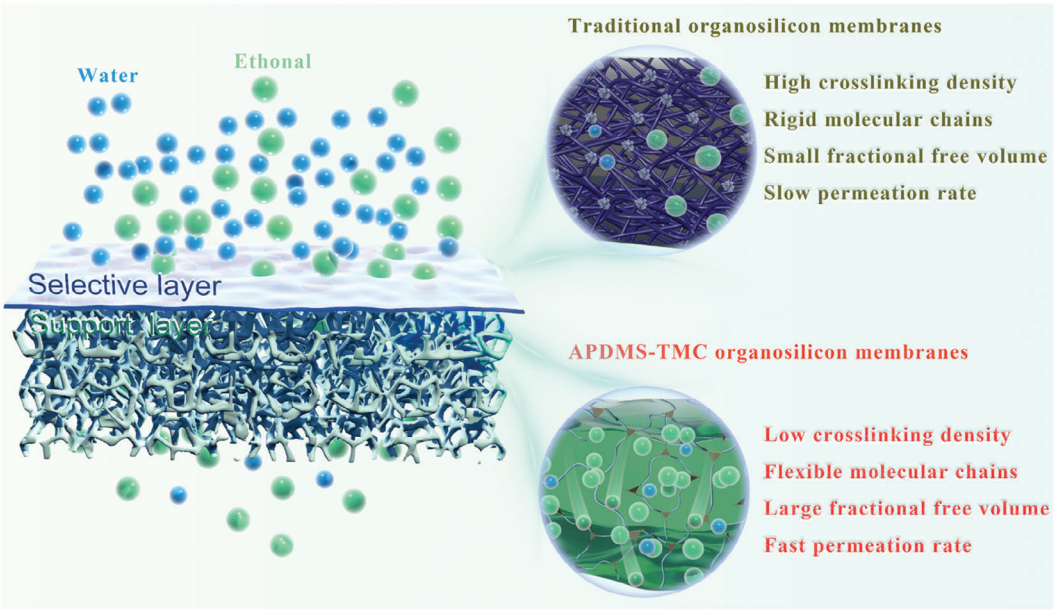

Figure 1. Schematic of the organosilicon membranes for the separation of alcohol–water mixtures. The separation mechanisms of traditional and APDMS-TMC organosilicon membranes and their advantages and disadvantages. The APDMS-TMC membrane with low crosslinking density exhibits flexible molecular chains, large FFV, and a fast permeation rate.

simple, reliable, and scalable method for the synthesis of high-performance organosilicon membranes remains a major challenge.

Herein, we present a rapid crosslinking method for the fabrication of high-performance and scalable organosilicon membranes with controllable crosslinking density for energy-efficient alcohol purification, using typical amide polymerization between bis(3-aminopropyl) terminated poly(dimethylsiloxane) (APDMS) macromer and a highly reactive crosslinker (trimethyl chloride, TMC). In our approach, the casting solution may be prepared within 30 min and stored for a long time (up to 75 days), challenging the traditional understanding of organosilicon membrane preparation. Typically, the preparation of casting solutions for traditional organosilicon membranes takes more than 5 h, and the prepared solution can be stored for less than 10 h. Therefore, the proposed approach is more suitable for scalable manufacturing than traditional methods. Moreover, our approach allows for quick and precise regulation of the crosslinking density within the organosilicon membrane, resulting in ultrahigh total flux (5.8 $kg{\cdot}m^{-2}{\cdot}h^{-1}$) and excellent separation factor (8.7) in ethanol purification. The underlying separation mechanism was explored via experiments and simulations. The results revealed that the membrane with low crosslinking density exhibits higher chain flexibility, larger fractional free volume (FFV), and weaker interactions between feed molecules and molecular chains than that with high crosslinking density. These characteristics result in the rapid and selective transport of alcohol molecules over water molecules within the organosilicon membrane, as depicted in **Figure 1**. Additionally, the membrane's low-cost and straightforward fabrication process also highlights its scalability for practically industrial applications.

2. Results and Discussion

2.1. Synthesis and Characterizations of Organosilicon Membranes

Organosilicon membranes were prepared through a facile solution-casting method (see Section A of Supporting Information).[12] Novel APDMS-TMC organosilicon membranes with an area of ≈411 cm^2 (Figure S1, Supporting Information) were synthesized via typical amide polymerization between the APDMS macromer and a highly reactive crosslinker, TMC (Figure S2, Supporting Information). The membranes are denoted as APDMS-TMC-*x*:*y* membranes, where *x*:*y* is the APDMS/TMC mass ratio. The chemical structures of the resulting APDMS-TMC membranes were verified by Fourier transform infrared spectroscopy (FTIR, Figure S7a, Supporting Information) and X-ray photoelectron spectroscopy (XPS, Figure S7b, Supporting Information). For comparison, traditional organosilicon membranes such as tetraethyl orthosilicate (TEOS)-crosslinked hydroxy-terminated PDMS (HPDMS) and commercial PDMS Sylgard 184 membranes were fabricated and denoted as HPDMS-TEOS-10:1 and PDMS 184-10:1, respectively, where 10:1 represents routine PDMS/crosslinker mass ratio.

The APDMS-TMC-403:1 (with a high PDMS/crosslinker mass ratio of 403:1) membrane exhibits markedly superior properties across several metrics compared to traditional PDMS 184-10:1 and HPDMS-TEOS-10:1 membranes (**Figure 2**a). Specifically, the APDMS-TMC-403:1 membrane demonstrates a higher total flux of 3.3 $kg{\cdot}m^{-2}{\cdot}h^{-1}$, a 453% increase over the PDMS 184-10:1 membrane's 0.6 $kg{\cdot}m^{-2}{\cdot}h^{-1}$ (Figure 2b). Furthermore, it exhibits a 35% higher separation factor (8.8) than the PDMS 184-10:1

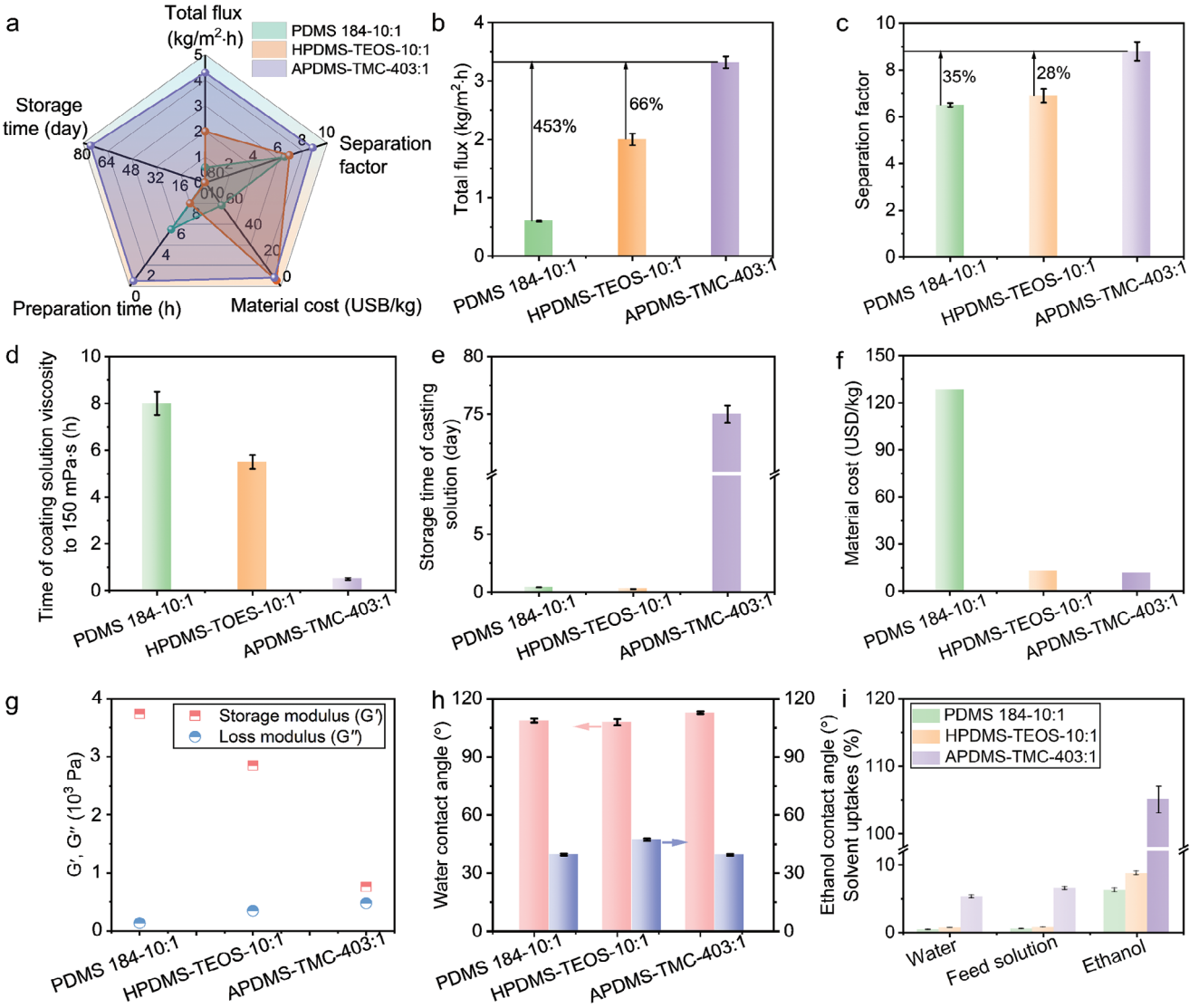

Figure 2. Superior properties of the APDMS-TMC organosilicon membranes. a) Radar plots of various properties and parameters, b) total fluxes, c) separation factors, d) preparation time of casting solutions, e) storage time of casting solutions, f) material cost, g) storage modulus (G′) and loss modulus (G″), h) water and ethanol contact angles, and i) solvent uptakes of the PDMS 184-10:1, HPDMS-TEOS-10:1, and APDMS-TEOS-403:1 membranes. Notably, the viscosity of the casting solution reaches 150 mPa·s, implying to the successful preparation of the casting solution. The data in Figure 2b–i are presented as mean ± standard deviation ($n = 3$).

membrane (6.5, Figure 2c). In terms of preparation, the APDMS-TMC-403:1 casting solution requires 15 times shorter preparation time than the PDMS 184-10:1 casting solution (Figure 2d), even though the former has substantially lower crosslinker content (1/403 of PDMS macromer amount) than the latter (1/10 of PDMS macromer amount). Additionally, the APDMS-TMC-403:1 casting solution can be stored for up to 75 days (Figure S8, Supporting Information) without significant viscosity change, whereas the conventional PDMS 184-10:1 solution must be used within 10 h because the excess of crosslinking agent causes a continuous increase in viscosity (Figure 2e). The APDMS-TMC-403:1 membrane also has ≈10.4 times lower material cost (≈11.3 USD/kg) than the PDMS 184-10:1 membrane (≈128.3 USD/kg) (Figure 2f and Table S2, Supporting Information), making it advantageous for large-scale production. These properties confirm the high separation performance and scalability of the APDMS-TMC membranes.

The notably superior separation performance of the APDMS-TMC membranes can be attributed to their unique inherent properties, as detailed in the results of various analyses (Figure 2g–i). The flexibility of the molecular chains within the membrane is a key parameter affecting the transport rate of feed molecules,[13] as confirmed by dynamic rheological properties (Figure 2g). Furthermore, the hydrophobicity of the membrane surface determines its organophilicity,[14] as substantiated by the measured water and ethanol contact angles (Figure 2h). Additionally, the sorption capability of the membrane toward ethanol molecules was evidenced by the tested solvent uptake

(Figure 2i).[15] These above properties affect the sorption and diffusion properties of the membranes, thereby contributing to their enhanced separation performance.

Specifically, for dynamic rheological properties, the APDMS-TMC-403:1 membrane exhibits the lowest storage modulus (G′) and the highest loss modulus (G″) compared to traditional PDMS 184-10:1 and HPDMS-TEOS-10:1 membranes (Figure 2g), indicating the greater flexibility of molecular chains. Differential scanning calorimetry (DSC) analysis further confirms such flexibility, as the APDMS-TMC-403:1 membrane shows the lowest glass transition temperature (−123.5 °C) compared to traditional PDMS 184-10:1 and HPDMS-TEOS-10:1 membranes (−117.6 and −120.3 °C, respectively) (Figure S9, Supporting Information). Additionally, the phase angle (δ) and loss factor (tan δ = G″/G′) indicate that the APDMS-TMC-403:1 membrane is viscoelastic, whereas the PDMS 184-10:1 and HPDMS-TEOS-10:1 membranes are elastic (Figure S10, Supporting Information). These major findings are explained by the low crosslinking density of the APDMS-TMC-403:1 membrane (Figure S11, Supporting Information). For the membrane surface hydrophobicity (Figure 2h), the APDMS-TMC-403:1 membrane exhibits the largest water contact angle and the smallest ethanol contact angle compared to traditional PDMS 184-10:1 and HPDMS-TEOS-10:1 membranes, indicating its greater hydrophobicity and organophilicity. Solvent uptake tests (Figure 2i) show that the APDMS-TMC-403:1 membrane exhibits the largest solvent uptake in the same solvent, indicative of a larger FFV. Notably, the membrane shows the strongest ethanol uptake in feed solution and ethanol solvent, suggesting a stronger affinity toward ethanol molecules owing to greater hydrophobicity and organophilicity. It is also demonstrated by the preferential ethanol sorption ability of the APDMS-TMC membrane in 5 wt% ethanol feed solution (Figure S12, Supporting Information). Whereas, the membrane's greatest water uptake is largely attributed to flexible chain segments that can increase chain movement in water, thereby leading to a larger swelling degree.

The notably superior scalability of the APDMS-TMC membranes can be attributed to their rapid crosslinking process, as demonstrated by the viscosity evolution and density functional theory (DFT) calculations (Figures S13–S15, Supporting Information). This high reactivity enables the rapid establishment of the appropriate crosslinking density in the APDMS-TMC systems. Notably, the reaction rate constant in the APDMS-TMC system is approximately nine orders of magnitude higher than that in the conventional HPDMS-TEOS system, facilitating the production of high-performance and scalable APDMS-TMC organosilicon membranes within a shorter timeframe.

2.2. Formation Conditions of Organosilicon Membranes

To explore the formation conditions of organosilicon membranes, we systematically investigated the effects of membrane materials, including the APDMS/TMC mass ratio, molecular weight of the APDMS macromer, and coupling agent. The mass ratio of the macromer to the coupling agent determines the crosslinking density of the resulting organosilicon membrane, thereby affecting the membrane formation ability and separation performance. The results indicate that the optimal range of APDMS/TMC mass ratio for the formation of APDMS-TMC membranes is between 357:1 and 463:1. This range ensures that the viscosity of the casting solution remains within suitable limits to avoid casting solution penetration into the substrate due to excessively low viscosity (Figure S16, Supporting Information), or insufficient flowability for film casting caused by overly high viscosity (Table S1, Supporting Information). The viscosities of the resulting casting solutions range from 46.5 to 3200 mPa·s (Table S1, Supporting Information), corresponding to crosslinking densities from $1.06 \times$ to 2.92×10^{-4} mol·mL^{-1} (**Figure 3a**). As illustrated in Figure 3b, the resulting APDMS-TMC membranes exhibit ultrahigh total fluxes, up to ≈3.3 kg·m^{-2}·h^{-1}, and acceptable ethanol/water separation factors (≈8.8), ascribed to the low crosslinking density resulted from the suitable APDMS/TMC mass ratio. In addition, as the APDMS/TMC mass ratio decreases from 463:1 to 357:1, the ethanol/water separation factors of the resulting membranes initially increase and then stabilize, attributed to the enhanced membrane elasticity (Figure S17, Supporting Information); while the total fluxes exhibit the opposite trend, originated from the reduced FFV with higher crosslinking densities (Figure 3a), suggesting that the solution-diffusion mechanism dominates the separation performance. In summary, appropriate APDMS/TMC mass ratios (403:1 – 357:1) are required to achieve the suitable crosslinking density (1.41×10^{-4} – 2.92×10^{-4} mol·mL^{-1}, Figure 3a) and excellent separation performance (total flux of ≈3.3 kg·m^{-2}·h^{-1} and ethanol/water separation factor of ≈8.8) in the prepared APDMS-TMC membranes.

The molecular weight of the APDMS macromer is another crucial factor influencing the crosslinking densities of the organosilicon membranes with the same APDMS/TMC mass ratio, thereby impacting the membrane formation ability and separation performance. Figure 3c shows that the viscosities of the APDMS-TMC casting solutions, prepared using APDMS macromers with molecular weights of 50 or 30 kDa (with APDMS/TMC mass ratio of 403:1 as a representative), are ≈150 mPa·s, indicative of good membrane formation ability (Table S1, Supporting Information). In contrast, the APDMS-TMC casting solutions prepared using APDMS macromers with lower molecular weights (2.5, 5, or 10 kDa) exhibit significantly lower viscosities (≈6 mPa·s), rendering membrane formation impractical (Figure S16, Supporting Information). This disparity is attributed to the macromers with higher molecular weight (50 or 30 kDa) forming integrated crosslinking networks, while low-molecular-weight macromers (2.5, 5, or 10 kDa) form only small micelles, as illustrated in the inserts of Figure 3c. Optical observations of APDMS-TMC casting solutions (Figure S18a–e, Supporting Information) support this hypothesis: light beams unobstructedly pass through solutions prepared with 50 or 30 kDa APDMS macromers, whereas solutions with APDMS macromers of lower molecular weights scatter light owing to micelle formation. FTIR spectra of the APDMS-TMC casting solution validate this phenomenon (Figure S19a, Supporting Information). The peak at 1660 cm^{-1}, assigned to the –C═O stretching vibration in amide groups, gradually increases in intensity with a decrease in the molecular weight of APDMS macromers. This indicates a higher crosslinking density in the solution prepared with APDMS macromers of lower molecular weight, due to their higher –NH_2 content (Figure S19b, Supporting Information), which leads to micelle formation rather than the

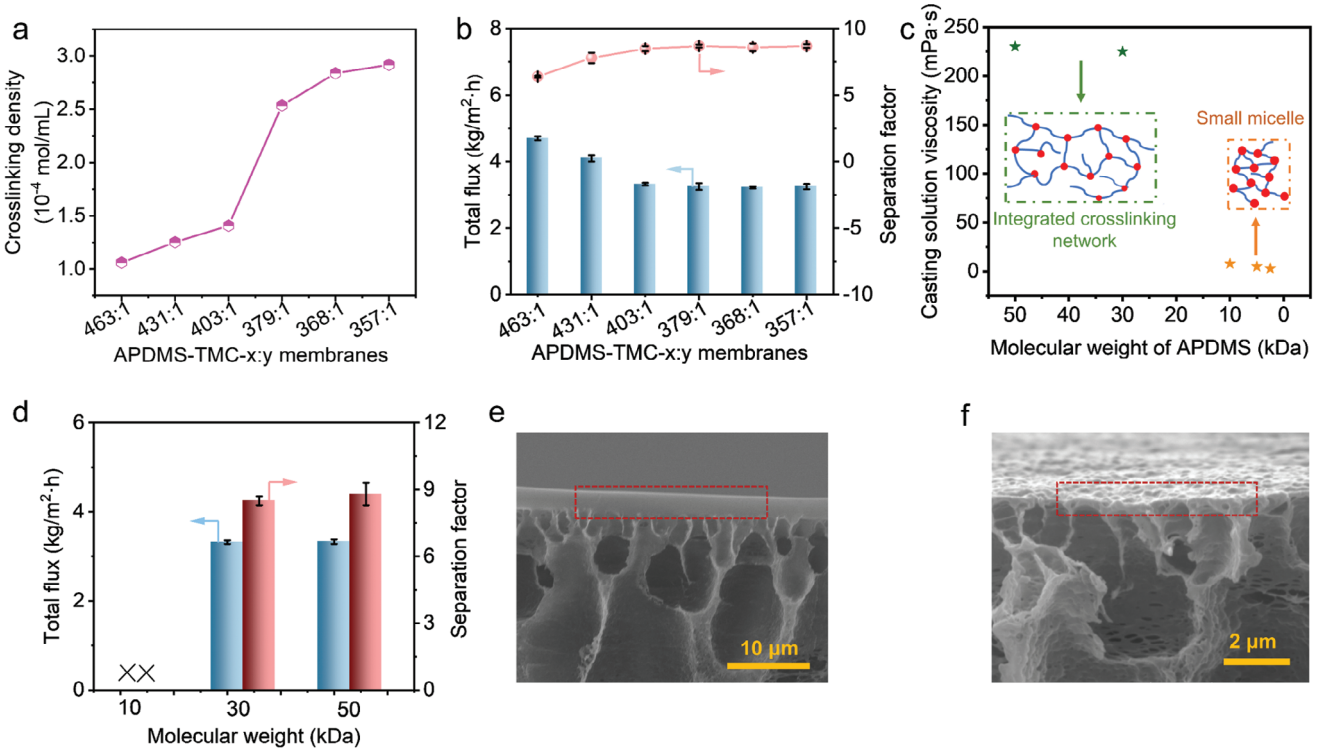

Figure 3. Formation condition of organosilicon membranes. a) Crosslinking densities of APDMS-TMC-*x*:*y* membranes. b) Total fluxes and ethanol/water separation factors of APDMS-TMC-*x*:*y* membranes. c) Viscosities of APDMS-TMC casting solutions obtained through the amide polymerization between TMC and APDMS with different molecular weights (inset: schematic structures of a small micelle and an integrated crosslinking network). d) Total fluxes and ethanol/water separation factors of APDMS-TMC-403:1 membranes prepared using APDMS macromers of different molecular weights (10, 30, or 50 kDa). Cross-sectional morphologies of e) APDMS-TMC-403:1 and f) APDMS-IPC-403:1 membranes. The data in Figure 3b–d are presented as mean ± standard deviation ($n = 3$).

formation of integrated crosslinking networks. Additionally, the effect of the molecular weight of APDMS macromers on the membrane pervaporation performance was investigated (Figure 3d). The APDMS-TMC-403:1 membrane prepared only with 30 or 50 kDa APDMS macromers is available and exhibits similar separation performance, probably attributed to the comparable crosslinking densities (Figure S20a, Supporting Information) and molecular chains flexibility (Figure S20b, Supporting Information), stemming from similar amine contents of the two APDMS macromers (Figure S19b, Supporting Information).

The coupling agent with three or more crosslinking sites is a prerequisite for the formation of a crosslinked APDMS network with end functional groups. This was confirmed using the viscosities of the casting solutions with different coupling agents. TMC, possessing three acyl chloride groups, acts as the coupling agent that crosslinks APDMS macromers, forming a casting solution with a viscosity of ≈150 mPa·s (Table S1, Supporting Information). Contrastingly, isophthaloyl chloride (IPC), featuring two acyl chloride groups, was used to connect APDMS macromers (Figure S4, Supporting Information). However, the viscosity of the prepared APDMS-IPC-403:1 casting solution does not significantly increase, and remains at ≈6 mPa·s, owing to the formation of a linear structure through the amide polymerization between APDMS and IPC (Figure S4, Supporting Information). The difference in viscosity directly influences membrane formation. Cross-sectional morphologies reveal that the APDMS-TMC-403:1 yields a continuous selective layer (Figure 3e), indicating successful membrane formation. In contrast, the APDMS-IPC-403:1 fails to form such a layer (Figure 3f) owing to its low viscosity: it penetrates into the substrate, preventing the formation of a continuous membrane structure with selective permeation properties. This indicates that the use of a coupling agent with three or more crosslinking sites, such as TMC, is essential for the preparation of APDMS crosslinked network with end functional groups and thereby for the fabrication of membranes with desired selective properties.

2.3. Universality of low Crosslinking Mechanism for Preparing High-Performance Organosilicon Membranes

The superior alcohol transport performance of APDMS-TMC organosilicon membranes is associated with their low crosslinking densities and high molecular chain flexibility. To verify this, we investigated the universality of the low crosslinking mechanism for the preparation of high-performance organosilicon membranes using different organosilicon systems. We employed a conventional HPDMS macromer along with triethoxyphenylsilane (TEPS) as the crosslinker, chosen for its chemical similarity to TMC (Figure S5, Supporting Information). The crosslinking densities of the resulting HPDMS-TEPS-*m*:*n* membranes were

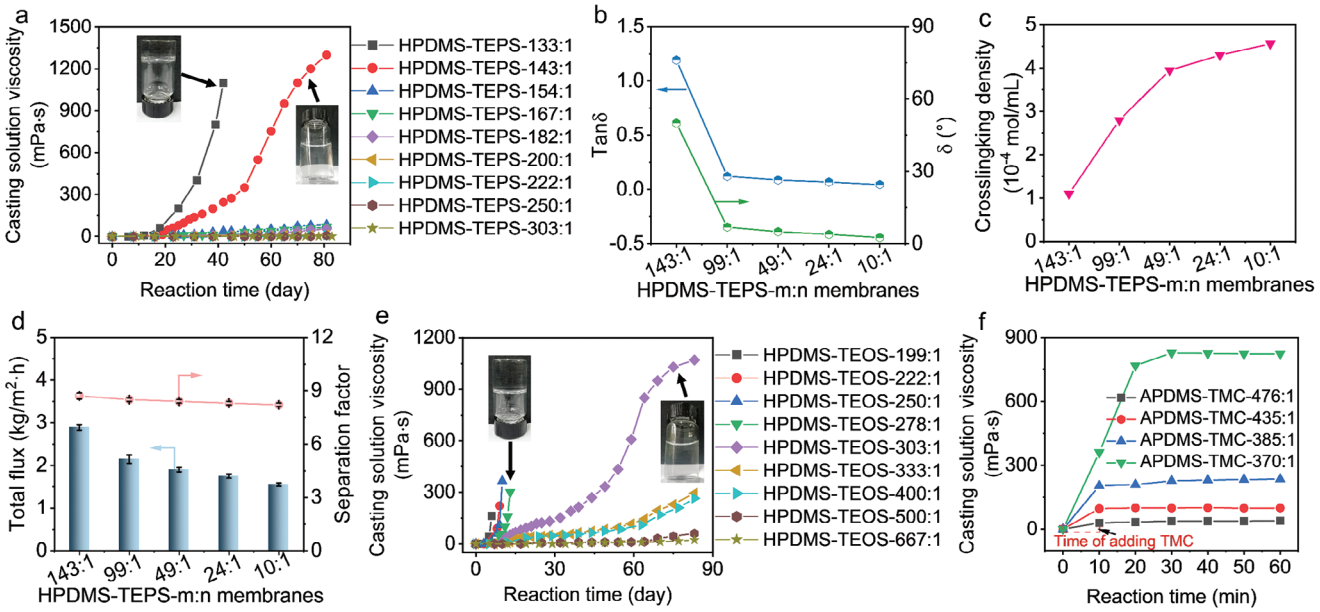

Figure 4. The universality of low crosslinking mechanism for the preparation of high-performance organosilicon membranes. a) Changes in viscosity of HPDMS-TEPS-*m*:*n* casting solutions over time (inset: the state of the casting solutions). b) tan δ and δ values, c) crosslinking densities, and d) total fluxes and separation factors of HPDMS-TEPS-*m*:*n* membranes. e) Changes in viscosity of HPDMS-TEOS-*e*:*f* casting solutions over time (inset: the state of the casting solutions). f) Changes in viscosity of APDMS-TMC-*x*:*y* casting solutions over time. The data in Figure 4d is presented as mean ± standard deviation ($n = 3$).

adjusted by varying the HPDMS/TEPS mass ratios (*m*:*n* = 10:1 – 303:1). The results show that the viscosities of the HPDMS-TEPS-*m*:*n* casting solutions with sufficient crosslinker content (*m*:*n* < 143:1) gradually increase over time, with solutions solidifying after 40 days (**Figures** 4a and S21, Supporting Information), indicating good membrane formation ability before solidifying. Furthermore, when the crosslinker content is sufficiently low, the HPDMS-TEPS-143:1 casting solution remains in a flowing state, exhibiting an increasing viscosity of up to 1300 mPa·s after an 81-day crosslinking reaction (Figure 4a), also indicative of good membrane formation ability (Table S1, Supporting Information). However, at ratios exceeding 143:1, the viscosities of the casting solutions stay low (<85 mPa·s) even after an 81-day crosslinking reaction (Figure 4a), suggestive of inferior membrane formation ability (Table S1, Supporting Information), probably due to the low crosslinking density. Dynamic rheological properties of HPDMS-TEPS membranes (Figure 4b) confirm the relationship between molecular chain flexibility and crosslinking density: as the HPDMS/TEPS mass ratio decreases, both the tan δ and δ values gradually decrease, implying reduced molecular chain flexibility owing to increased crosslinking density (Figure 4c). Subsequently, the alcohol purification performance of HPDMS-TEPS-*m*:*n* membranes with various HPDMS/TEPS mass ratios was tested using a 5 wt% ethanol aqueous solution at 60 °C (Figure 4d) to verify the relationship between molecular chain flexibility and separation performance. As the HPDMS/TEPS mass ratio decreases, the total fluxes of the resultant membranes gradually decrease, attributed to reduced molecular chain flexibility (Figure 4b), while the ethanol/water separation factors remain almost unchanged. The HPDMS-TEPS-143:1 membrane, with the lowest crosslinking density (1.1×10^{-4} mol·mL^{-1}), exhibits the highest total flux (2.9 kg·m^{-2}·h^{-1}) and a comparable separation factor (8.7).

Similarly, the crosslinking densities of traditional HPDMS-TEOS-*e*:*f* membranes were also regulated by adjusting the HPDMS/TEOS mass ratios (*e*:*f* = 10:1 – 667:1). The trend in viscosity for HPDMS-TEOS casting solutions (Figure 4e) mirrors that for HPDMS-TEPS solutions (Figure 4a). At an HPDMS/TEOS mass ratio of 303:1, the formed casting solution exhibits low viscosity (1070 mPa·s) and crosslinking density (1.12×10^{-4} mol·mL^{-1}) after an 83-day crosslinking reaction. Notably, the crosslinking density of the HPDMS-TEOS-303:1 membrane is lower approximately three times than that of conventional HPDMS-TEOS-10:1 membrane (4.71×10^{-4} mol·mL^{-1}), resulting in a 60% improvement in the total flux, reaching 3.2 kg·m^{-2}·h^{-1}, while maintaining a stable ethanol/water separation factor (≈8.7). These results are attributed to the high flexibility of molecular chains caused by the low crosslinking density.

The findings highlight the feasibility of the production of high-performance organosilicon membranes using both HPDMS-TEOS and HPDMS-TEPS systems with appropriate low crosslinking density. This approach suggests that similar high-performance membranes could also be developed by other polysiloxane macromers like vinyl-terminated PDMS or PDMS 184, provided that suitable crosslinking agents and appropriate crosslinking densities are employed. This versatile methodology expands the potential application scope of the membranes, enabling the tailoring of molecular chain flexibility to address specific industrial or scientific requirements. Furthermore, it can be also found from Figures 4a–e that the decrease in the amount of crosslinker agents (TEPS and TEOS) significantly slows the curing time of PDMS casting solutions, thereby extending their

storage time when an appropriate amount of crosslinker is used. However, the newly developed APDMS-TMC system significantly reduces the preparation time of casting solutions: APDMS-TMC system requires only 30 min (Figure 4f), whereas the traditional HPDMS-TOES system requires 83 days (Figure 4e). This improvement is attributed to the rapid crosslinking rate between APDMS and TMC (Figure S15, Supporting Information), highlighting the excellent suitability of this system for industrial applications where efficiency and time management are critical.

Additionally, compared to the rapid increase in viscosity observed in the APDMS-TMC casting solution (Figure 4f), which indicates its facile controllability, the viscosities of HPDMS-TEPS and HPEMS-TEOS casting solutions increase at a much slower rate (Figures 4a,e), when the concentrations of crosslinkers are very low (less than 0.75% and 0.5%, respectively). However, when subjected to high crosslinker concentrations (e.g., 10% HPDMS), both systems exhibit a significant increase in viscosity. This poses challenges for industrial applications, as the resulting sticky casting solution (Figure S21, Supporting Information) hinders continuous membrane production. In contrast, the APDMS-TMC system demonstrates both a rapid and complete reaction, leading to viscosity stabilization once cross-linking process is nearly complete. This allows for easier management of the casting solution's viscosity by carefully controlling the amount of TMC, thereby enhancing its suitability for industrial applications.

2.4. Separation Mechanism of High-Performance Organosilicon Membranes

Our experimental data have confirmed that decreasing the crosslinking density significantly enhances the alcohol purification performance of organosilicon membranes due to increased molecular chain flexibility. However, the molecular mechanisms underlying the relationship between molecular chain flexibility and separation performance are not yet fully understood. To delve deeper into this relationship, molecular dynamics (MD) simulations were employed to elucidate the molecular-level differences between organosilicon membranes with low and high crosslinking densities (abbreviated as LCDM and HCDM, respectively), including aspects such as molecular chain flexibility, FFV, and interactions between solvent molecules and molecular chains. The highly reactive nature of TMC as a crosslinker makes it impractical to produce a highly crosslinked APDMS-TMC membrane by casting an APDMS-TMC solution. With low TMC content, a lightly crosslinked APDMS-TMC casting solution is immediately formed, resulting in an APDMS-TMC LCDM when knife-cast onto the substrate. In contrast, high TMC content leads to the formation of a highly crosslinked APDMS-TMC casting solution with poor flowability, preventing the formation of an APDMS-TMC HCDM. As an alternative approach, the HPDMS-TEOS system was chosen to study the molecular-level differences between LCDM and HCDM. Due to the low reactivity of the HPDMS-TEOS system, both LCDM and HCDM, depending on TEOS content, can be formed using this system. The construction procedure for the models of HPDMS-TEOS LCDM and HCDM is described in Section A of Supporting Information. As shown in Figure S22 (Supporting Information), the models of both HPDMS-TEOS HCDM and LCDM have the same thickness (Z-axis direction, 6.623 nm), while the sizes of the lateral dimensions are 2.579 × 2.663 and 3.502 × 1.987 nm, respectively.

Figures 5a and S23 (Supporting Information) depict the swelling behaviors of HPDMS-TEOS HCDM and LCDM in water, ethanol, and the feed solution used in this study (5 wt% ethanol aqueous solution). It is observed that HPDMS-TEOS LCDM exhibits a significantly higher swelling degree than HPDMS-TEOS HCDM in the same solvent, indicating greater molecular chain flexibility in LCDM owing to its lower crosslinking density, facilitating the rapid molecule transport across the membrane (Figure 2b). Additionally, the swelling degree of both LCDM and HCDM membranes in different liquids follows the order of ethanol > feed solution > water, indicating a stronger affinity of HPDMS-TEOS membranes toward ethanol molecules, which is conducive to selective separation of ethanol and water (Figure 2c).

Further investigation of HPDMS-TEOS HCDM and LCDM through MD simulations reveals notable differences between the microstructures. As illustrated in Figure 5b, whether before or after the membrane swelling, HPDMS-TEOS LCDMs consistently exhibit larger FFV than HPDMS-TEOS HCDMs, attributed to their lower crosslinking density. Correspondingly, HPDMS-TEOS LCDMs with larger FFV display lower densities (Figure S24a,b, Supporting Information) and higher solvent uptakes in the same solvent (Figure 5c) than HPDMS-TEOS HCDMs. Additionally, the simulated void size distribution (VSD) results (Figure 5d and Figure S24c, Supporting Information) reveal that HPDMS-TEOS LCDMs contain more large-sized voids than HPDMS-TEOS HCDMs. These simulation results positively impact the separation efficiency of alcohol from alcohol–water mixtures.

MD simulations were also used to explore the interactions between the penetrant molecules and polymer chains, crucial for the transport of the permeate molecules.[16] Results (Figure 5e) show that Van der Waals and Coulomb interaction energies in the HPDMS-TEOS LCDM are significantly lower than those in the HPDMS-TEOS HCDM, indicating the potential for faster transport of feed components through the LCDM. The simulated displacement trajectory of ethanol molecules through membranes confirms this (Figure 5f), indicating faster ethanol transport through the LCDM (0.8 ns) than through the HCDM (1.9 ns). These findings underscore that the lower crosslinking density of the HPDMS-TEOS LCDM increases molecular chain flexibility, FFV, and void size distribution, thereby improving alcohol separation efficiency in membrane applications.

2.5. Practical Application Potential of Organosilicon Membranes

To demonstrate the universal applicability of the developed APDMS-TMC membranes in various liquid mixture systems, their separation capabilities for purifying other alcohols were explored. Thanks to its superior properties (Figure 2a), the APDMS-TMC-403:1 membrane was selected as a representative specimen for further optimization. **Figure** 6a demonstrates that the APDMS-TMC-403:1 membrane achieves ultrahigh total flux (>3.0 $kg \cdot m^{-2} \cdot h^{-1}$) and satisfactory separation factors (>6.4) for C1 – C4 alcohol aqueous feed solutions. Notably, despite the larger molecular size of *n*-butanol compared to other alcohols,[17]

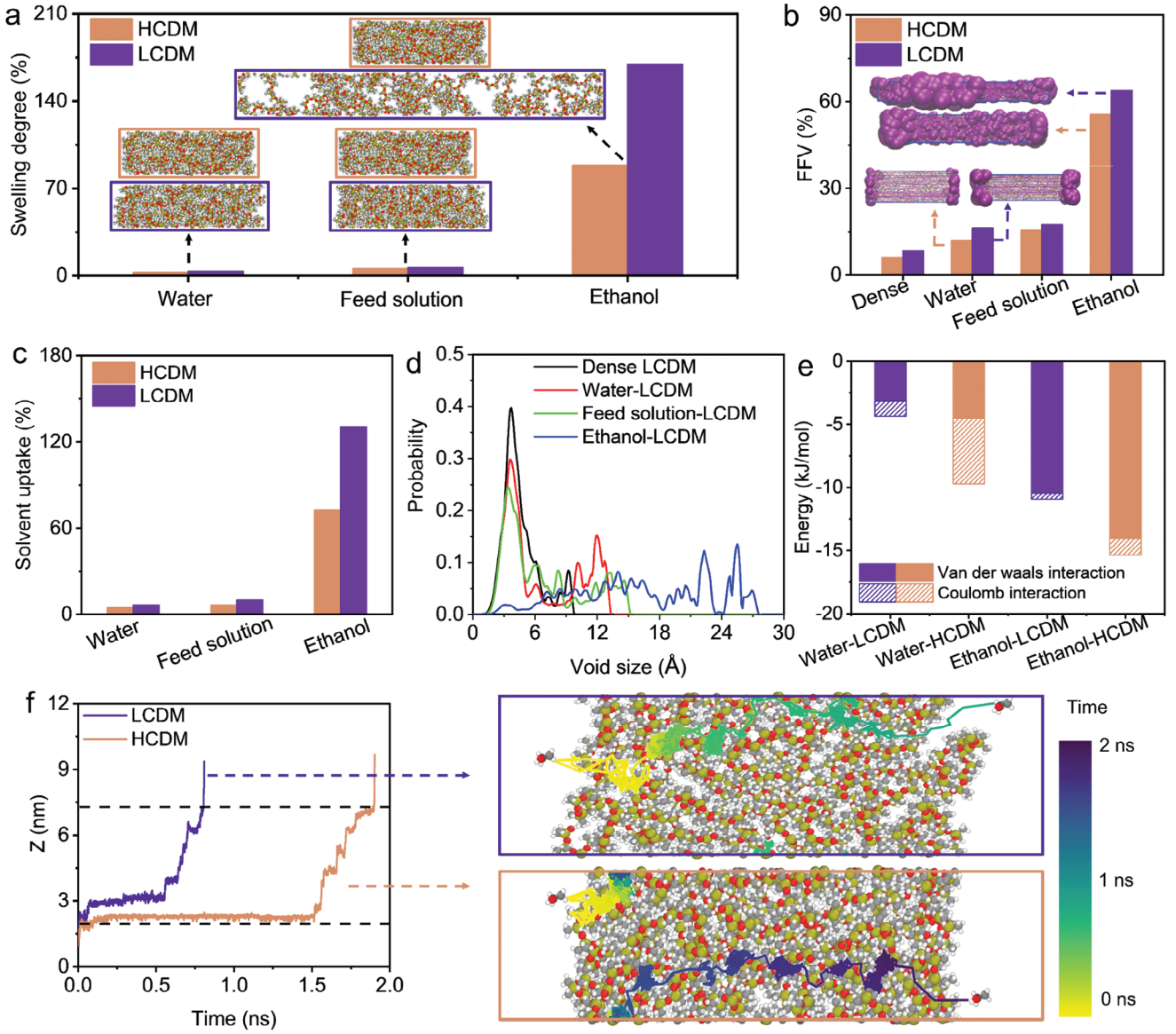

Figure 5. MD simulation results. a) Swelling degrees and snapshots of the HPDMS-TEOS HCDM and LCDM before and after swelling in water, feed solution, and ethanol. b) FFV and pore channels (purple sphere) of the HPDMS-TEOS HCDM and LCDM before and after swelling in water, feed solution, and ethanol. c) Solvent uptakes of the HPDMS-TEOS HCDM and LCDM in water, feed solution, and ethanol. d) The void size distribution (VSD) of the HPDMS-TEOS LCDM before and after swelling in water, feed solution, and ethanol. e) Van der Waals and Coulomb interaction energies between water/ethanol molecules and molecular chains in the HPDMS-TEOS HCDM and LCDM. f) The displacement trajectory of ethanol molecules through HPDMS-TEOS HCDM and LCDM along the Z-axis (HPDMS-TEOS membrane was fixed and the region between the two dotted lines represents the thickness of the membrane.) Atoms: Hydrogen (white), Oxygen (red), Carbon (grey), and Silicon (chartreuse).

the membrane exhibits higher flux (5.3 $kg \cdot m^{-2} \cdot h^{-1}$) and separation factor (12) for *n*-butanol feed solution. This can be attributed to two main reasons. First, the Hildebrand solubility parameter of *n*-butanol (23.2 $MPa^{1/2}$) is closer to that of PDMS (15.5 $MPa^{1/2}$) than those of the other three alcohols—methanol (29.6 $MPa^{1/2}$), ethanol (26.5 $MPa^{1/2}$), and isopropanol (23.6 $MPa^{1/2}$),[18] indicating a stronger affinity toward *n*-butanol molecules and better sorption on the membrane surface. Second, the molecular polarities of alcohols follow the order of methanol > ethanol > isopropanol > *n*-butanol. Larger alcohol molecules with lower molecular polarity exhibit weaker interactions with molecular chains, resulting in higher permeation rates through the membrane.[13,19] For comprehensive performance benchmarking, we compared the pervaporation performances of various polymeric-based membranes and the APDMS-TMC-403:1 membrane for C1 – C4 alcohol purification, as shown in Figure 6b and Tables S3–S6 (Supporting Information). The results demonstrate that the APDMS-TMC-403:1 membrane achieves ultrahigh total flux and comparable separation factor for C1 – C4 alcohol purification, surpassing most state-of-the-art polymeric-based membranes. It stands out due to its high chain flexibility and large FFV from low crosslinking density, facilitating alcohol molecule

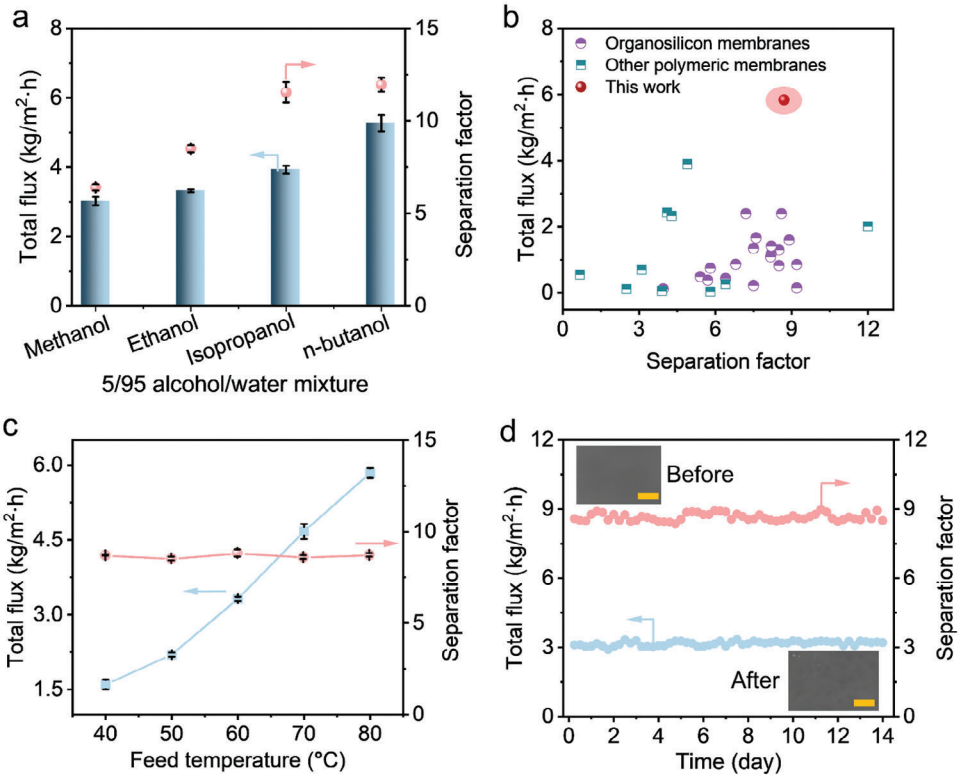

Figure 6. Practical application potential of the prepared organosilicon membrane. a) APDMS-TMC-403:1 membrane for the recovery of different alcohols with a 5 wt% alcohol aqueous solution at 60 °C. b) Comparison of APDMS-TMC-403:1 studied in this work with polymeric-based pervaporation membranes for ethanol recovery (Details are provided in Table S4, Supporting Information.). The inset refers to SEM surface images of the membrane before and after the long-term test (scale bar: 1 µm). c) Effect of feed temperature on the total flux and separation factor of the APDMS-TMC-403:1 membrane using a 5% ethanol aqueous feed solution. d) Long-term stability of the APDMS-TMC-403:1 membrane. The data in Figure 6a–c are presented as mean ± standard deviation ($n = 3$).

transport and resulting in a higher total flux. The results underline the potential of APDMS-TMC organosilicon membranes in alcohol purification applications.

To assess the practical application potential of the organosilicon membranes, we measured their mechanical properties by tensile experiment. As shown in Figure S25 (Supporting Information), the APDMS-TMC-403:1 membrane exhibits a larger strain compared to both the PVDF substrate and conventional HPDMS-TEOS-10:1 membrane. This enhanced strain can be attributed to the flexible chain segments in the membrane with a low crosslinking density (1.41×10^{-4} mol·mL^{-1}). Interestingly, despite its low crosslinking density, the APDMS-TMC-403:1 membrane demonstrates an elongation stress comparable to that of the HPDMS-TEOS-10:1 membrane which has a higher crosslinking density (4.71×10^{-4} mol·mL^{-1}). This indicates that the APDMS-TMC-403:1 membrane possesses similar mechanical strength, highlighting its potential for practical applications. Furthermore, we investigated the membrane stability through pervaporation tests at various conditions, including higher operating temperatures and a prolonged duration. As depicted in Figure 6c, increasing feed temperature from 40 to 80 °C results in a significant 258% increase in the total flux from 1.6 to 5.8 kg·m^{-2}·h^{-1}, while the ethanol/water separation factor remains consistent (≈8.6), indicating superior performance and stability even at elevated temperatures. The increase in the total flux is primarily ascribed to the higher chain flexibility and driving force at elevated temperatures.[20] Moreover, the essentially constant separation performance of the APDMS-TMC-403:1 membrane over a 14-day test verifies its excellent stability (Figure 6d). Before and after the long-term test, the membrane exhibits a smooth and intact surface (inset in Figure 6d), also suggesting its excellent stability. In addition, the selective layer thickness also affects the stability of the membrane through altering the swelling behavior of the membrane during the pervaporation test. Therefore, an optimal thickness (2.5 µm) of the selective layer benefited a higher separation performance (Figure S26 and Table S7, Supporting Information), because the actual separation layer was located beneath the selective layer during the pervaporation test owing to its swelling as reported in a previous study.[21]

3. Conclusions

In summary, we have developed a novel high-performance and scalable organosilicon membrane through amide polymerization between APDMS macromer and TMC, designed to facilitate fast and selective transport of alcohol molecules form alcohol–water mixtures. The proposed APDMS-TMC organosilicon membrane demonstrated lower crosslinking density and higher molecular chain flexibility than the traditional HPDMS-TEOS and PDMS 184 organosilicon membranes. The

precise selection of the APDMS/TMC mass ratio (ranging from 403:1 to 357:1), the molecular weight of the APDMS macromer (50 or 30 kDa), and coupling agent (TMC, rather than IPC) ensured good film formation ability and stable separation performance of the prepared APDMS-TMC membrane. Compared to the organosilicon membrane with high crosslinking density, the organosilicon membrane with low crosslinking density possessed more flexible molecular chains and a larger FFV, as well as weaker interactions between feed molecules and molecular chains, all of which are beneficial for fast and selective alcohol purification. The resulting APDMS-TMC-403:1 membrane exhibited an ultrahigh total flux (5.8 $kg{\cdot}m^{-2}{\cdot}h^{-1}$) and a comparable separation factor (8.7), surpassing most state-of-the-art polymeric-based membranes for ethanol purification. Additionally, this APDMS-TMC-403:1 membrane demonstrated versatile purification ability for other C1–C4 alcohols (methanol, ethanol, isopropanol, and *n*-butanol). Its stable separation performance at higher operation temperatures and over extended periods, along with the stability of casting solution for long-term storage, and the ease and speed of membrane preparation, further confirmed its great potential for practical implementation. Notably, the use of appropriate crosslinking density can transform conventional organosilicon membranes into high-performance variants by using a suitable crosslinker and amount. Therefore, crosslinking engineering of organosilicon membranes paves the way for the development of next-generation membranes for energy-efficient molecular separations.

Supporting Information

Supporting Information is available from the Wiley Online Library or from the author.

Acknowledgements

The authors express their gratitude for the financial support received from National Natural Science Foundation of China (grant nos. 22378153 and 21878117) and the National Key Research and Development Program of China (grant no. 2020YFB1709301). Additionally, we would like to thank the Analysis and Testing Center, the Analysis and Testing Center of Chemistry and Chemical Engineering School (HUST) for conducting various characterization tests.

Conflict of Interest

The authors declare no conflict of interest.

Author Contributions

T.Z. and D.S. contributed equally to this work. Tengyang Zhu: conceptualization, data curation, formal analysis, investigation, methodology, visualization, writing-original draft, writing-review & editing; Dongchen Shen: data curation, investigation, writing-original draft; Jiayu Dong: data curation, investigation, writing-review & editing; Huan Liu: visualization and investigation; Qing Xia: formal analysis and investigation; Song Li: investigation, supervision, writing-review & editing; Lu Shao: investigation and methodology; Yan Wang: conceptualization, funding acquisition, investigation, methodology, project administration, supervision, writing-review & editing.

Data Availability Statement

The data that support the findings of this study are available in the supplementary material of this article.

Keywords

alcohol purification, chain flexibility, crosslinking engineering, organosilicon membrane

Received: August 21, 2024
Revised: November 18, 2024
Published online: December 1, 2024

[1] a) J. H. Kim, M. Cook, L. Peeva, J. Yeo, L. W. Bolton, Y. M. Lee, A. G. Livingston, *Energ. Environ. Sci.* **2020**, *13*, 4862; b) M. M. Thackeray, C. Wolverton, E. D. Isaacs, *Energ. Environ. Sci.* **2012**, *5*, 7854; c) J. C. Liao, L. Mi, S. Pontrelli, S. Luo, *Nat. Rev. Microbiol.* **2016**, *14*, 288; d) C. Beer, M. Reichstein, E. Tomelleri, P. Ciais, M. Jung, N. Carvalhais, C. Rödenbeck, M. Altaf Arain, D. Baldocchi, G. B. Bonan, A. Bondeau, A. Cescatti, G. Lasslop, A. Lindroth, M. Lomas, S. Luyssaert, H. Margolis, K. W. Oleson, O. Roupsard, E. Veenendaal, N. Viovy, C. Williams, F. I. Woodward, D. Papale, *Science* **2010**, *329*, 834; e) P. Fairley, *Nature* **2011**, *474*, S2; f) S. Sarp, S. G. Hernandez, C. Chen, S. W. Sheehan, *Joule* **2021**, *5*, 59.

[2] a) R. Dhabhai, C. H. Niu, A. K. Dalai, *Bioresour. Bioprocess.* **2018**, *5*, 1; b) S. Nishiyama, N. Kimura, T. Hirai, K. Nakagawa, T. Yoshioka, *Ind. Eng. Chem. Res.* **2023**, *62*, 14611; c) L. H. Xu, S. H. Li, H. Mao, Y. Li, A. S. Zhang, S. Wang, W. M. Liu, J. Lv, T. Wang, W. W. Cai, L. Sang, W. W. Xie, C. Pei, Z. Z. Li, Y. N. Feng, Z. P. Zhao, *Science* **2022**, *378*, 308.

[3] a) C. d. C. Nogueira, C. E. d. A. Padilha, J. M. d. M. Dantas, F. G. M. d. Medeiros, A. d. A. Guilherme, D. F. d. S. Souza, E. S. d. Santos, *Renew. Energ.* **2021**, *180*, 914; b) H. Fan, Q. Shi, H. Yan, S. Ji, J. Dong, G. Zhang, *Angew. Chem., Int. Ed.* **2014**, *53*, 5578; c) D. Yang, D. Tian, C. Xue, F. Gao, Y. Liu, H. Li, Y. Bao, J. Liang, Z. Zhao, J. Qiu, *Nano Lett.* **2018**, *18*, 6150; d) J. A. Stoeger, J. Choi, M. Tsapatsis, *Energ. Environ. Sci.* **2011**, *4*, 3479.

[4] a) S. Sikiru, K. J. Abioye, H. B. Adedayo, S. Y. Adebukola, H. Soleimani, M. Anar, *Renew. Sustain. Energ. Rev.* **2024**, *200*, 114535; b) E. V. Silva, J. L. F. Alves, G. D. Mumbach, G. F. Reus, R. A. F. Machado, A. Bolzan, C. Marangoni, *J. Ind. Eng. Chem.* **2024**, *135*, 480; c) K. Dudek, I. Valdez-Vazquez, J. Koop, *Sep. Purif. Technol.* **2022**, *297*, 121551.

[5] a) L. H. Xu, Y. Li, S. H. Li, H. Mao, Z. P. Zhao, *Chem. Eng. J.* **2024**, *490*, 151606; b) M. Yang, J. J. Zhu, A. L. McGaughey, R. D. Priestley, E. M. V. Hoek, D. Jassby, Z. J. Ren, *Environ. Sci. Technol.* **2024**, *58*, 10128; c) B. Mo, Y. Jin, G. Zhou, G. Liu, C. Chen, Z. Liu, G. Liu, W. Jin, *AIChE J* **2024**, *70*, e18368; d) J. Xiao, T. Zhu, H. Zhang, W. Xie, R. Dong, Y. Li, X. Wang, *Angew. Chem., Int. Ed.* **2024**, *63*, 202411270.

[6] a) J. H. Huang, Y. Q. Zhang, J. Guo, F. Yang, J. Ma, Y. P. Bai, L. Shao, S. M. Liu, H. Wang, *Nat. Sustain.* **2024**, *7*, 901; b) X. Chen, S. Mohammed, G. Yang, T. Qian, Y. Chen, H. Ma, Z. Xie, X. Zhang, G. P. Simon, H. Wang, *Adv. Mater.* **2020**, *32*, 2002320.

[7] a) W. M. Liu, X. R. Chen, H. Mao, S. H. Li, Y. M. Zhang, L. H. Xu, Z. P. Zhao, *J. Membr. Sci.* **2024**, *704*, 122889; b) D. Song, C. Li, J. Li, T. Cao, P. Cai, N. Wang, Q. F. An, *J. Membr. Sci.* **2024**, *696*, 122529.

[8] a) G. E. Wang, G. Xu, *Sci. Bull.* **2022**, *67*, 2381; b) Z. Si, H. Wu, P. Qin, B. Van der Bruggen, *Sep. Purif. Technol.* **2022**, *298*, 121612.

[9] a) Z. Si, J. Li, L. Ma, D. Cai, S. Li, J. Baeyens, J. Degreve, J. Nie, T. Tan, P. Qin, *Angew. Chem., Int. Ed.* **2019**, *131*, 17335; b) Y. Pan, Y. Guo, J. Liu, H. Zhu, G. Chen, Q. Liu, G. Liu, W. Jin, *Angew. Chem., Int. Ed.* **2021**, *61*, 202111810.

[10] X. L. Liu, Y. S. Li, G. Q. Zhu, Y. J. Ban, L. Y. Xu, W. S. Yang, *Angew. Chem., Int. Ed.* **2011**, *50*, 10636.
[11] P. P. Li, U. Shareef, Z. L. Xu, D. Taymazov, Y. Z. Wu, Y. S. Xu, *J. Membr. Sci.* **2022**, *641*, 119937.
[12] a) Q. Yin, K. Pang, Y. N. Feng, L. Han, A. Morsali, X. Y. Li, T. F. Liu, *Nat. Commun.* **2024**, *15*, 634; b) C. Li, Y. Jiang, Z. Wu, Y. Zhang, C. Huang, S. Cheng, Y. You, P. Zhang, W. Chen, L. Mao, L. Jiang, *Angew. Chem., Int. Ed.* **2022**, *62*, 202215906; c) Y. Su, S. Cong, M. Shan, Y. Zhang, *AlChE J* **2021**, *68*, e17410.
[13] T. Zhu, J. Dong, H. Liu, Y. Wang, *Mater. Horiz.* **2023**, *10*, 3024.
[14] X. He, T. Wang, J. Huang, J. Chen, J. Li, *Sep. Purif. Technol.* **2020**, *241*, 116675.
[15] H. Mao, H. G. Zhen, A. Ahmad, A. S. Zhang, Z. P. Zhao, *J. Membr. Sci.* **2019**, *573*, 344.
[16] a) T. Zhu, Q. Xia, J. Zuo, S. Liu, X. Yu, Y. Wang, *Adv. Membr.* **2021**, *1*, 100008; b) Y. K. Ong, G. M. Shi, N. L. Le, Y. P. Tang, J. Zuo, S. P. Nunes, T. S. Chung, *Prog. Polym. Sci.* **2016**, *57*, 1.
[17] Z. Si, G. Li, Z. Wang, D. Cai, S. Li, J. Baeyens, P. Qin, *ACS Appl. Mater. Interfaces* **2020**, *12*, 31887.
[18] P. Weerachanchai, K. H. Lim, J. M. Lee, *Bioresour. Technol.* **2014**, *156*, 404.
[19] W. D. Zhang, W. Sun, J. Yang, Z. Q. Ren, *Appl. Biochem. Biotechnol.* **2009**, *160*, 156.
[20] a) T. Zhu, S. Xu, F. Yu, X. Yu, Y. Wang, *J. Membr. Sci.* **2020**, *598*, 117681; b) T. Zhu, X. Yu, M. Yi, Y. Wang, *ACS Sustain. Chem.Eng.* **2020**, *8*, 12664.
[21] Y. Wang, L. Jiang, T. Matsuura, T. S. Chung, S. H. Goh, *J. Membr. Sci.* **2008**, *318*, 217.